Phonons in two-dimensional colloidal crystals with bond-strength disorder

Matthew D. Gratale,[1] Peter J. Yunker,[1,2,3] Ke Chen,[4] Tim Still,[1] Kevin B. Aptowicz,[5] and A. G. Yodh[1]

[1]*Department of Physics and Astronomy, University of Pennsylvania, Philadelphia, Pennsylvania 19104, USA*
[2]*New England Biolabs Inc., 240 County Road, Ipswich, Massachusetts 01938, USA*
[3]*School of Engineering and Applied Sciences Department of Physics, Harvard University, Cambridge, Massachusetts 02138, USA*
[4]*Beijing National Laboratory for Condensed Matter Physics and Key Laboratory of Soft Matter Physics, Institute of Physics, Chinese Academy of Sciences, Beijing 100190, China*
[5]*Department of Physics, West Chester University, West Chester, Pennsylvania 19383, USA*

We study phonon modes in two-dimensional colloidal crystals composed of soft microgel particles with hard polystyrene particle dopants distributed randomly on the triangular lattice. This experimental approach produces close-packed lattices of spheres with random bond strength disorder, i.e., the effective springs coupling nearest neighbors are very stiff, very soft, or of intermediate stiffness. Particle tracking video microscopy and covariance matrix techniques are then employed to derive the phonon modes of the corresponding "shadow" crystals with bond strength disorder as a function of increasing dopant concentration. At low frequencies, hard and soft particles participate equally in the phonon modes, and the samples exhibit Debye-like density of states behavior characteristic of crystals. For mid- and high-frequency phonons, the relative participation of hard versus soft particles in each mode is found to vary systematically with dopant concentration. Additionally, a few localized modes, primarily associated with hard particle motions, are found at the highest frequencies.

Macroscopic properties of disordered materials often differ from those of their crystalline counterparts [1–4], and the search for the microscopic origin of these differences is an interesting and ongoing enterprise [5–12]. A variety of disordered solids, ranging from metallic to colloidal glasses, have been found to exhibit similar vibrational properties [13–22]. Notable among these features is the so-called "boson peak," corresponding to an excess number of low-frequency phonon modes compared to Debye predictions for crystals [23], and the presence of floppy, quasilocalized modes [24–31]. Thus far, most of this research has focused on materials wherein the microscopic constituents are *structurally* disordered. Structurally disordered solids typically form from rapidly quenched atomic and molecular liquids [32,33] and, in the case of colloids, from densely packed rapidly loaded and/or polydisperse suspensions [1,2,24,34–43].

Besides structural disorder, other kinds of disorder are present in nature. Disorder can be introduced into a crystalline material, for example, via heterogenous interactions or bonds between constituent particles [44]. Interestingly, simulations and numerical studies suggest that similarities and differences exist between systems with pure structural disorder versus bond disorder [45–49], but experimental studies of such systems are lacking. Further, because the simulations and numerical studies have primarily focused on the shape of the density of states, e.g., in searches for insight into the origin of the boson peak, little is known about the behavior of the individual particles that make up such systems. Thus, experiments that derive information about individual particle motions can provide complementary insights and can help to elucidate similarities and differences between structurally disordered versus bond-interaction disordered systems, including their relationship to underlying ordered phases.

To this end, we study and report on the vibrational properties of colloidal crystals with bond disorder confined in quasi-two-dimensional chambers. These colloids are composed primarily of soft poly(N-isopropylacrylamide) (PNIPAM) microgel particles, with hard polystyrene (PS) particle dopants distributed randomly on the lattice. Importantly, soft and hard spheres in the crystal have the same diameter. As a result, 2D structurally ordered lattices are produced with a distribution of bond strengths; nearest-neighbor bonds are either very stiff, very soft, or of intermediate stiffness. Video microscopy is employed to track the motion of all particles, and particle displacement covariances are used to derive the phonon modes of the corresponding "shadow" crystals with the same geometric configuration and interactions as the experimental colloidal system, but absent damping. Thus, we explore the phonon modes in crystals with bond strength disorder as a function of increasing dopant concentration.

The experiments reveal that the vibrational density of states in bond strength disordered crystals is modified by doping with small numbers of especially stiff particles. However, these bond disordered crystals were not found to exhibit the classic phonon behavior of structurally disordered glasses. For example, the low-frequency Boson peak is not apparent in any of the samples studied. Nevertheless, the shape of the phonon density of states (DOS), and the relative participation of hard versus soft particles in each mode, is found to vary systematically in the intermediate- and high-frequency phonon ranges. At low frequencies, all samples exhibit phonon DOS with Debye law scaling characteristic of crystalline systems; additionally, both hard and soft particles participate equally in these low-frequency phonon modes. At intermediate frequencies, the phonon DOS exhibits a regime with numbers of modes per unit frequency clearly in excess of Debye scaling predictions, and the characteristic frequency of the high-frequency regime decreases with increasing dopant concentration. Interestingly, intermediate modes recruit greater participation of soft particles, while high-frequency modes
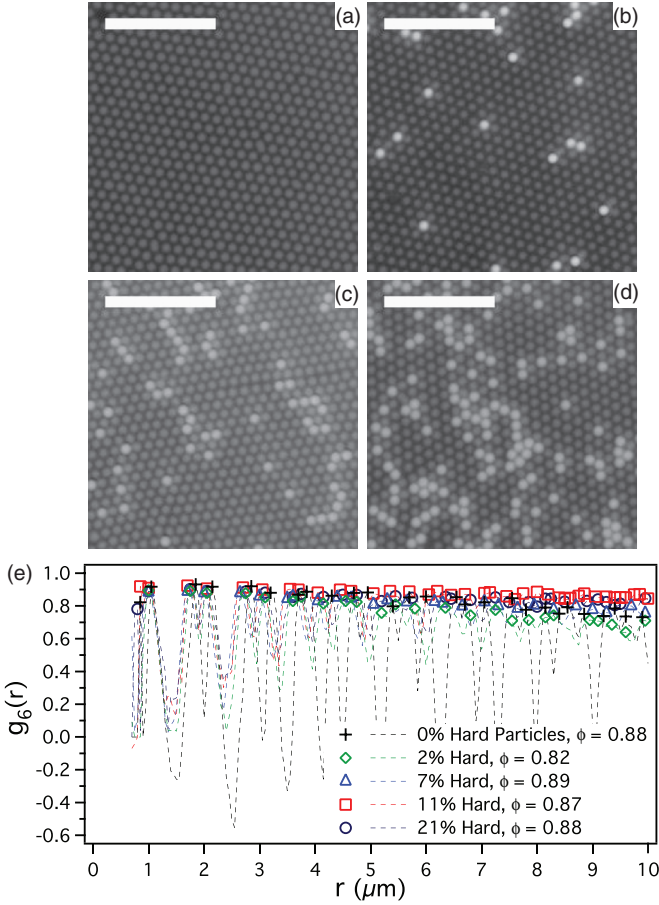
FIG. 1. (Color online) Images of a soft PNIPAM particle colloidal crystal doped with (a) 0%, (b) 2%, (c) 11%, and (d) 21% hard polystyrene (PS) particles. The white spheres are PS particles, and the gray spheres are PNIPAM particles. Scale bars are $10\,\mu$m. (e) The orientational correlation function, $g_6(r)$, of all crystals studied. Symbols represent local maxima and the dashed lines represent the full correlation function.

recruit greater participation of hard particles. Thus, three frequency regimes are identified. Low frequencies feature soft and hard particles behaving similarly; intermediate frequencies are dominated by soft particle motions, and high frequencies are dominated by hard particle motions.

The experiments employed ensembles of particles sandwiched between a glass slide and cover slip (Fisher Scientific), creating a quasi-2D chamber (Fig. 1). Polystyrene (PS) particles (Invitrogen) had a diameter of 1.1 μm and the poly(N-isopropylacrylamide) (PNIPAM) particles [50] had a diameter of $\sim$1.1 μm. Because of this similarity in size, the particle mixture readily self-assembled into a triangular crystal. PNIPAM particles have a soft interparticle potential [51], while polystyrene particles are much more hard-sphere-like [52–54]. Since two different species of particles are employed, i.e., soft PNIPAM and hard polystyrene, three different interparticle interaction combinations arise (soft-soft, soft-hard, and hard-hard). A small amount of Fluorescein dye ($\sim$0.2% w/v, Sigma-Aldrich) was added to the aqueous suspension of particles in order to improve imaging contrast. The dye was excited using light from a mercury lamp that was directed through a 488-nm wavelength bandpass filter;

the resulting video images consisted of dark particles on a bright background.

To characterize the triangular crystalline order of the samples, the orientational and translational correlation functions, $g_6(r)$ and $g_T(r)$, respectively, were calculated for all of the crystals; $g_\alpha(r = |\mathbf{r_i} - \mathbf{r_j}|) = \langle \psi_{\alpha i}^*(\mathbf{r_i})\psi_{\alpha j}(\mathbf{r_j})\rangle$, where r_i and r_j are the positions of particles i and j, and $\alpha = 6, T$. ψ_{6i} and ψ_{6j} are, thus, the orientational order parameters for particles i and j, and ψ_{Ti} and ψ_{Tj} are the translation order parameters for particles i and j. The orientational and translational order parameters for a given particle j are defined as $\psi_{6j} = (\sum_{k=1}^{nn} e^{6i\theta_{jk}})/nn$, where θ_{jk} is the angle between particle j and its neighbor k and nn is the number of nearest neighbors, $\psi_{Tj} = e^{i\mathbf{G}\cdot\mathbf{r_j}}$, where $\mathbf{G}$ is a primary reciprocal lattice vector determined from the peak in the sample's 2D structure factor, $s(k)$. Notice in Fig. 1(e), the orientational correlation function $g_6(r)$ is large (>0.8) at short distances and does not significantly decay over the longer distances probed; this observation suggests that the samples possess good triangular order. Measurements of the translational correlation functions $g_T(r)$ (discussed more fully in the Supplemental Material [55]) lead to similar conclusions about long-range crystalline order in the samples. Briefly, for the 0%, 11%, and 21% hard-particle crystals, $g_T(r)$ behaved similar to $g_6(r)$. $g_T(r)$ for the 2% and 7% hard-particle crystals decayed more quickly at longer distances, but this effect was brought about by a single grain boundary present in the field of view of these two crystals. We separately confirmed, with studies of crystal subsections excluding the grain boundaries, that the phonon behavior of the smaller subsections was consistent with that derived from the larger fields of view, including the grain boundaries.

We thus create crystals with three distinct interparticle potentials distributed randomly on the triangular lattice. Particle motion was recorded using video microscopy, while the samples were kept at a temperature of 25°C using an objective heater (Bioptechs) connected to the microscope oil immersion objective. Video data of $N_{\text{tot}} \approx 1000$–1500 particles was recorded at a rate of 60 frames per second for 500 seconds. The raw images (dark particles on a bright background) were then inverted to yield images of bright particles on a dark background (Fig. 1), and the motion of all particles was extracted using standard particle tracking techniques [56].

We derive the vibrational properties of the doped crystals using the displacement covariance matrix method [24,35,57]–[59]. Briefly, we measure $\mathbf{u}(t)$, the $2N_{\text{tot}}$-component vector of the displacements of all particles from their average positions $(\bar{x}, \bar{y})$. Then we compute the time-averaged displacement covariance matrix (covariance matrix), $C_{ij} = \langle u_i(t)u_j(t)\rangle_t$, where $i, j = 1, ..., 2N_{\text{tot}}$ run over particles and positional coordinates, and the average runs over time (i.e., over all frames). In the harmonic approximation, the covariance matrix C is directly related to the sample's stiffness matrix K, defined as the matrix of second derivatives of the effective pair interaction potential with respect to particle position displacements; in particular, $(C^{-1})_{ij}k_BT = K_{ij}$. The vibrational properties of the so-called shadow system, a system of particles with the same static properties as our experimental system (i.e., with the same covariance and stiffness matrices, C and K), but absent damping, are derived from the dynamical matrix D,
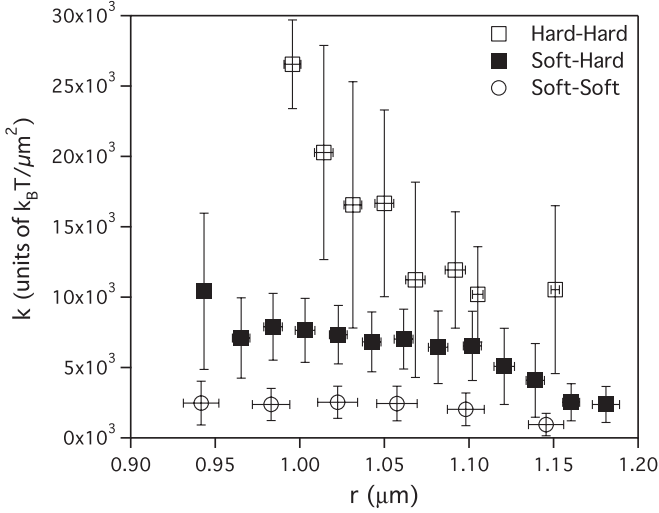
FIG. 2. Effective spring constants k between two hard particles (hollow squares), two soft particles (circles), and hard-particle–soft-particle pairs (filled squares) derived from the computed spring constant matrix K as a function of average particle separation r for the 21% hard-particle doped crystal.

FIG. 3. (Color online) Accumulated mode number, $N(\omega)$, for all doped crystals and pure PNIPAM crystal as a function of the frequency ω scaled by the minimum frequency $\omega_{\min}$ for each sample. The solid black line represents Debye law scaling, $N(\omega) \sim \omega^2$. The accumulated mode numbers are logarithmically binned.

which is directly related to the stiffness matrix with $D_{ij} = K_{ij}/m_{ij}$, where $m_{ij} = \sqrt{m_i m_j}$ with m_i the mass of particle i. Diagonalizing the dynamical matrix gives the eigenvalues and eigenvectors of the shadow system phonons. The eigenvalues correspond to the frequencies, ω, of the phonon modes, while the eigenvectors correspond to the particle amplitudes associated with each of the phonon modes. Extraction of the phonons of an undamped system from a damped system, such as ours, is possible as long as the damping is only a direct function of the particle momenta. In this case, the displacement covariance and spring constant matrices, C and K, respectively, only depend on the static interactions between particles, which are the same for the real and shadow systems. For further discussion about the limitations of this approach, see Refs. [18,59]– [62].

From the spring constant matrix K, it is apparent that three distinct nearest-neighbor springs are present, corresponding to the three nearest-neighbor particle combinations. Figure 2 shows the effective spring constants measured in the 21% hard-particle crystal. Notice that hard-hard particle pairings have the stiffest springs, soft-soft particle pairings have the softest springs, and soft-hard particle pairings have springs with an intermediate stiffness.

For a 2D crystal, the Debye model predicts that the accumulated number of phonon modes, $N(\omega)$, should grow as the frequency squared in the low-frequency regime [63]. Note, $N(\omega)$ is defined as the number of modes with frequency less than or equal to ω and is thus integral over the phonon DOS. In Fig. 3 the measured $N(\omega)$ is plotted for all doped crystals (2%, 7%, 11%, 21% PS/hard particles), as well as for a pure PNIPAM crystal (0% PS/hard particles). At low frequencies, $N(\omega)$ exhibits similar scaling with frequency in all crystals. This scaling is very close to the Debye model prediction. Thus, despite different degrees of bond strength disorder, the low-frequency DOS behavior is quite similar to that of a perfect crystal.
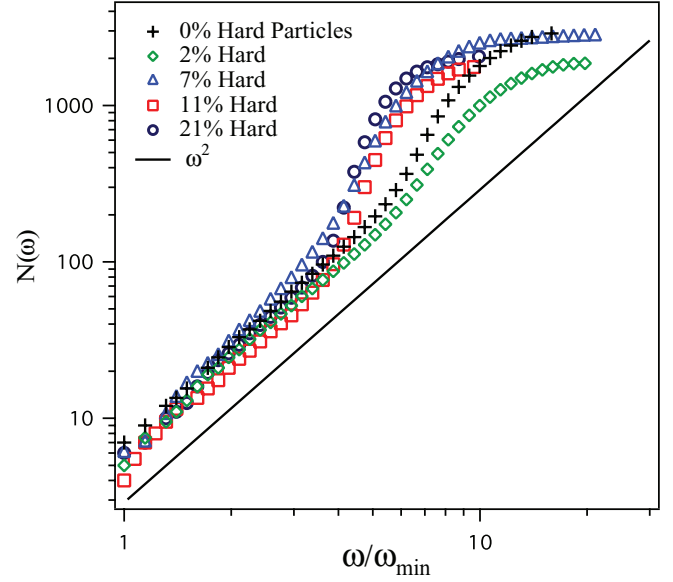
At intermediate frequencies $N(\omega)$ grows faster than predictions of the Debye model, and at the highest frequencies, $N(\omega)$ plateaus. Note, a somewhat similar DOS behavior at low-intermediate frequencies was also observed by Kaya *et al.* [57] using two-dimensional slices within a three-dimensional colloidal crystal; they attributed this deviation from Debye behavior to a heterogeneous distribution of microgel particle stiffness and argued that the deviations were related to the boson peak. Our low-frequency data, however, does not support the existence of a boson peak in these systems. To better understand how crystalline behavior is preserved at low frequencies, as well as to elucidate the behaviors exhibited by these systems at higher frequencies, we utilize the derived eigenvectors of the present system to obtain spatial information about the phonon modes.

First, we quantify the contributions of soft and hard particles to each mode. This information is derived by calculating the participation fractions of each species for each mode. The eigenvectors of each mode have components (i.e., associated displacement amplitudes) corresponding to each particle and each direction, i.e., $\mathbf{e}(\omega) = [e_{1x}(\omega), ..., e_{N_{\text{tot}}x}(\omega), e_{1y}(\omega), ..., e_{N_{\text{tot}}y}(\omega)]$, where N_{tot} is the total number of particles in the sample. Further, all eigenvectors are normalized such that $|\mathbf{e}(\omega)| = \sum_{\alpha}[e_{\alpha x}^2(\omega) + e_{\alpha y}^2(\omega)] = 1$, where α runs over all particles. The participation fraction for particle α in a mode with frequency ω is, therefore, given by $P_{F,\alpha}(\omega) = e_{\alpha x}^2(\omega) + e_{\alpha y}^2(\omega)$. Thus, the participation fraction of hard spheres in a mode with frequency ω is $P_{F,\text{Hard}} = \sum_{h}[e_{hx}^2(\omega) + e_{hy}^2(\omega)]$, where h is the set of indices corresponding to hard spheres in the eigenvector, and the participation fraction of soft spheres is $P_{F,\text{Soft}}(\omega) = 1 - P_{F,\text{Hard}} = \sum_{s}[e_{sx}^2(\omega) + e_{sy}^2(\omega)]$, where s is the set of indices corresponding to soft spheres in the eigenvector.
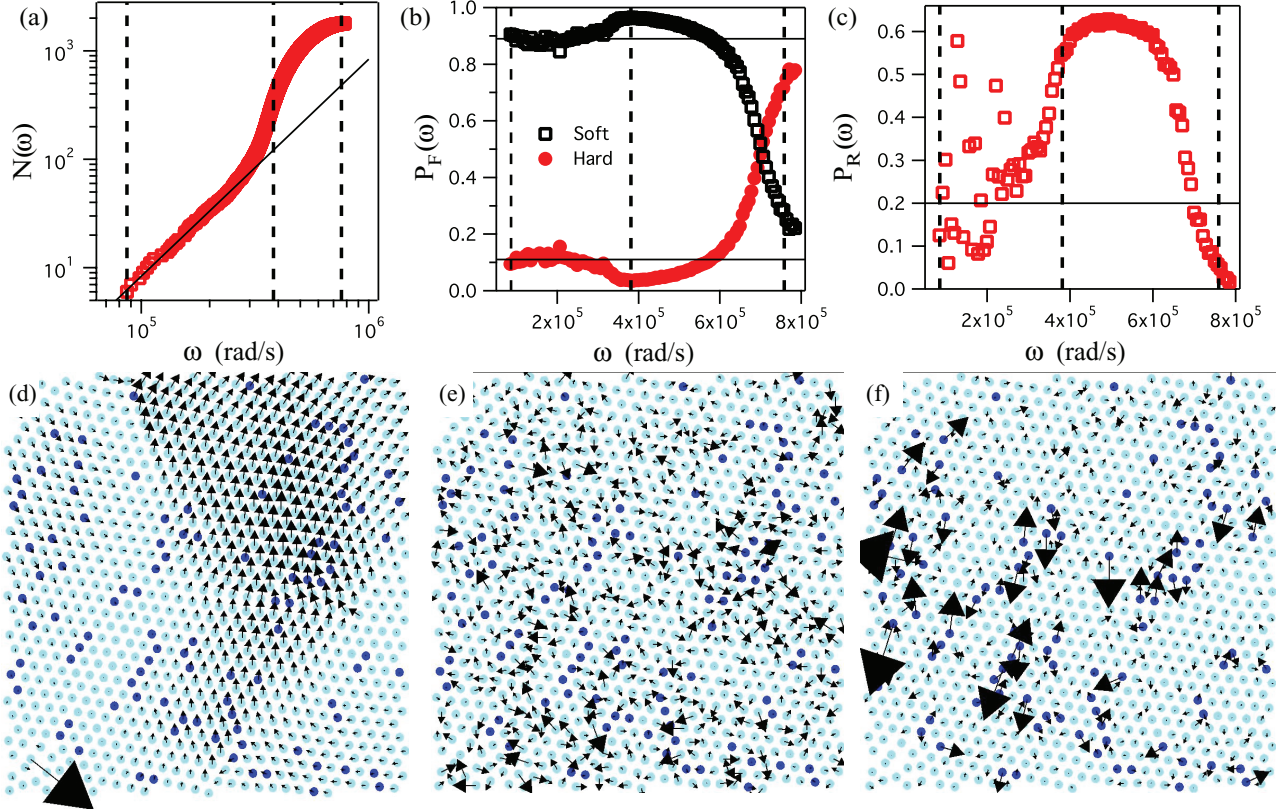
FIG. 4. (Color online) Mode characterization and representation for 11% hard-particle crystal. (a) Accumulated mode number $N(\omega)$ with solid black line representing Debye law scaling, $N(\omega) \sim \omega^2$, and dotted black lines show where representative modes (d–f) are found on plot. (b) Participation fraction $P_F(\omega)$ of hard (filled red circles) and soft (hollow black squares) spheres. Horizontal solid black lines show number fractions of soft and hard particles, 89% and 11%, respectively, and dashed black lines again show representative modes. The participation fraction of hard and soft spheres is binned (i.e., averaged) over a bin size of 20×10^3 rad/s. (c) Participation ratio $P_R(\omega)$ with solid black line showing threshold for localized versus extended motion, and dotted lines again show representative modes. The participation ratio of all particles is binned over a bin size of 20×10^3 rad/s. (d–f) Vector displacement plots of representative modes (d) $\omega = 86.4 \times 10^3$ rad/s, (e) $\omega = 381.2 \times 10^3$ rad/s, and (f) $\omega = 758.7 \times 10^3$ rad/s. Dark blue dots are hard particles, light blue are soft particles, and arrows are the particles' displacements. The larger the arrow, the larger the particle's displacement.

Second, we quantify the spatial extent of each mode by calculating its participation ratio. The mode participation ratio is defined as $P_R(\omega) = [\sum_\alpha e_{\alpha x}^2(\omega) + e_{\alpha y}^2(\omega)]^2 / [N_{\text{tot}} \sum_\alpha e_{\alpha x}^4(\omega) + e_{\alpha y}^4(\omega)]$. A low numerical value for the participation ratio indicates that the mode is spatially localized, while a high value indicates the mode is spatially extended. The participation ratio cut-off used to separate localized from extended modes is typically set to be 0.2. Modes with a participation ratio below (above) 0.2 are considered localized (extended).

The general behavior of the bond-disordered crystals can be gleaned from Fig. 4, wherein representative phonon modes of an 11% hard-particle-doped crystal are shown, along with the accumulated mode number, $N(\omega)$, the participation fraction, $P_F(\omega)$, and the participation ratio, $P_R(\omega)$. Interestingly, at low frequencies, where Debye-like behavior was observed in the accumulated mode number, the participation fractions of hard and soft particles follow their respective number fractions in the sample, i.e., soft and hard particles participate equally [Fig. 4(b)]. This representative mode and other modes at low frequencies exhibit long-wavelength-like extended behavior; the behavior is similar to that of corresponding modes at

low frequencies in perfect crystals. Note, also, that a few low-frequency modes have very low participation ratios (i.e., they have at least some quasilocalized character); we believe these effects are probably due to lattice point defects and/or grain boundaries [64]. In the case of point defects, these low-frequency modes appear to possess both long-wavelength-like character and localized motions near lattice defects. The mode shown in Fig. 4(d) is an example of one such mode; notice the defect in the lower left-hand corner. Thus, though the participation ratio of such modes is typically below the expected participation ratio of extended modes ($\sim$0.5), they clearly exhibit a form of long-wavelength-like spatially extended behavior, too.

At intermediate frequencies, the accumulated mode number grows faster than would be expected should Debye scaling continue to higher frequencies. In addition, the motion in these modes is dominated by soft spheres as is best quantified by the participation fraction. In particular, we see that the participation fraction of soft spheres in these modes is higher than the number ratio of soft spheres in the system (Fig. 4(b)); i.e., we observe enhanced participation of soft spheres and diminished participation of hard spheres

compared to their sample number fractions. The motion of these intermediate modes is also spatially extended, but their character appears qualitatively different than was found at low frequencies.

The highest frequency modes are dominated by hard spheres. Specifically, a crossover in the participation fraction is observed wherein hard particles have enhanced participation, and the participation of soft spheres is diminished. The highest frequency modes do not display long wavelength extended behavior; rather, they appear to be more localized than most of the modes observed at intermediate and low frequencies. This latter effect is supported quantitatively by the participation ratio [Fig. 4(c)]. The participation ratio at intermediate frequencies is far above the 0.2 threshold. At high frequencies, however, the participation ratio drops below 0.2.

We next explore the effects of differing dopant concentrations. To better compare samples with different dopant concentrations, we scale the frequencies of each sample type by its mean frequency $\langle\omega\rangle$. In this manner, we can plot the behaviors of all samples over the same relative frequency range to discern trends more easily. Further, by subtracting the number fraction of hard spheres in a sample from the measured participation fraction, i.e., $P_{F,\text{Hard}}(\omega) - N_{\text{Hard}}/N_{\text{tot}}$, we can suggestively plot all participation fraction versus frequency data as shown in Fig. 5. Here, when $P_{F,\text{Hard}}(\omega) - N_{\text{Hard}}/N_{\text{tot}}$ has a value of zero, then all particles participate equally (i.e., corresponding to their number fraction in the sample); a negative value means there is diminished participation by the hard spheres and enhanced participation by the soft spheres; a positive value means enhanced participation by the hard spheres and diminished participation by the soft spheres. The three frequency regimes observed in the 11% hard particle crystals are apparent in all doped crystals within this plotting scheme. Equal participation is observed at low frequencies, diminished hard-particle participation at intermediate frequencies, and enhanced hard-particle participation at high frequencies. In addition, we find that the extent (i.e., frequency range) of the high-frequency regime, wherein hard particles become the primary mode participants, shifts to lower relative frequency as the number of hard-particle dopants increases.

The participation ratio of all doped crystals and the pure soft PNIPAM crystal are also shown in Fig. 5 as a function of scaled frequency. Notice that extended modes predominate at low and intermediate frequencies for all crystals, regardless of dopant concentration. The high-frequency modes in the pure soft particle crystal are also observed to be extended; however, the highest frequency modes of all doped crystals are found to be localized. Evidently, the hard-particle dopants dominate motion at high frequencies, thus localizing vibrational motion since they are relatively isolated. This high-frequency behavior appears similar, at least superficially, to that observed in colloidal glasses [19,24].

To further confirm our findings, we studied computationally generated spring networks. These spring networks employed varying ratios of stiff and soft springs located randomly within the lattice. Part of our motivation for carrying out these simulations was due to the fact that the spatial distribution of hard-particle dopants in the experimental samples was not perfectly random; we therefore hoped to clarify whether this
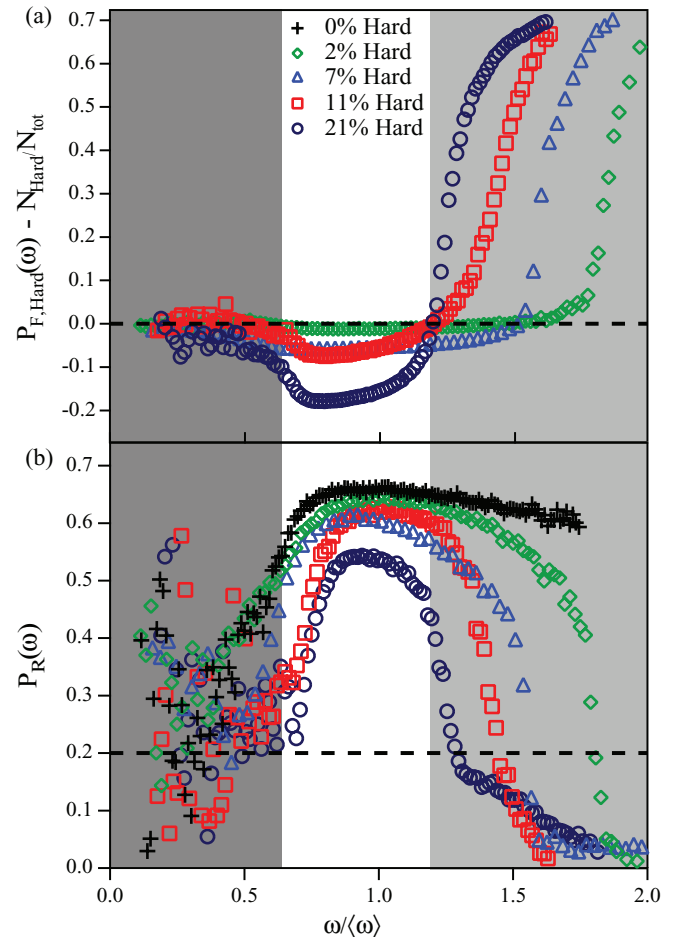

FIG. 5. (Color online) (a) Hard-particle participation fractions shifted by hard-particle number fractions $P_{F,\text{Hard}}(\omega) - N_{\text{Hard}}/N_{\text{tot}}$ as a function of frequency scaled by the mean frequency $\omega/\langle\omega\rangle$ for all doped crystals. Dotted line represents equal participation. (b) Participation ratio as a function of frequency scaled by the mean frequency $\omega/\langle\omega\rangle$ for all doped crystals as well as pure soft-particle crystal. Dotted line represents localized versus extended threshold. Legend is for both figures; however, data for 0% hard-particle crystal only in panel b. Both participation fraction and participation ratio data is binned (i.e., averaged) over a bin size of 20×10^3 rad/s.

lack of perfect randomness would affect any of the conclusions we made about the phonon spectra.

The computer simulations employed particles with equal masses on triangular lattices. The particles were randomly chosen to have one of two spring constants, k_1 or k_2. We set k_2 to be five times larger than k_1. Particles with spring constant k_2 are referred to as "stiff" and particles with spring constant k_1 are referred to as "soft." The effective spring between two neighboring particles is the mean value of the spring constants of the two particles. In other words, the effective spring constant k_{ij} between neighboring particles i and j is given by $k_{ij} = (k_i + k_j)/2$, where k_i and k_j are the spring constants of individual particles i and j, respectively. This model was employed to be consistent with our experiments, wherein two hard particles are coupled by an effectively stiff spring, two soft particles are coupled by an effectively soft spring, and hard-particle–soft-particle pairs are coupled by an effective
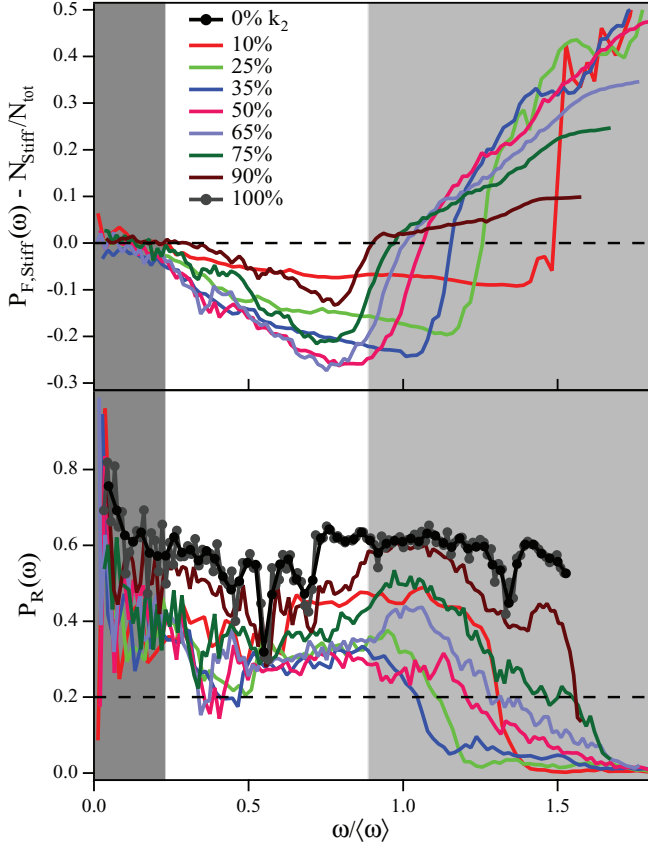
FIG. 6. (Color online) (a) Stiff-particle participation fractions shifted by stiff-particle number fractions $P_{F,\text{Stiff}}(\omega) - N_{\text{Stiff}}/N_{\text{tot}}$ as a function of frequency scaled by the mean frequency $\omega/\langle\omega\rangle$ for computationally generated springs networks, excluding those that are purely soft particles or purely stiff particles. Dotted line represents equal participation. (b) Participation ratio $P_R(\omega)$ as a function of frequency scaled by the mean frequency $\omega/\langle\omega\rangle$ for all computationally generated spring networks, including those that are purely soft particles (black line with dots) or purely stiff particles (gray line with dots). Dotted line represents localized versus extended threshold. Legend is for both figures; however, data for 0% and 100% stiff-particle crystal only in panel b.

spring of intermediate stiffness. All non-nearest-neighbor springs were set to zero. We thus generated a spring constant matrix K based on nearest-neighbor spring interactions; K, in turn, gives rise to a dynamical matrix D for the spring network. The eigenvalues and eigenvectors of D were calculated, and the frequencies, participation fractions, participation ratios, etc., were derived. One hundred different initial configurations were employed for each network; networks were chosen with 0, 10, 25, 35, 50, 65, 75, 90, and 100 percent stiff particles. By averaging over 100 iterations, we minimized effects specific to any one configuration.

Plots derived from these "computationally generated data," and analogous to those of the experimental data in Fig. 5, are provided in Fig. 6. Notice that the computationally generated networks exhibit the same three frequency regimes as the experimental systems. Further, the participation ratios, $P_R(\omega)$, of all computationally generated spring networks (0% to 100% stiff particles) exhibit trends similar to experiment. Thus, it

appears that the small nonrandomness in the experimental dopant spatial distribution does not introduce systematic errors that affect our primary conclusions.

In summary, the vibrational modes in soft-particle crystals doped with hard particles exhibit three distinct frequency regimes. At low frequencies, crystalline (Debye-like) behavior in the DOS is observed in all systems regardless of doping. These low-frequency modes display long wavelength behavior in which hard and soft particles participate equally. At intermediate frequencies, the modes are extended and dominated by soft particles. At the highest frequencies, the modes are more localized and dominated by hard particles. Our computationally generated spring networks exhibit many of the trends observed here and even extrapolate to higher number fractions of hard spheres.

The experimental results imply that while the introduction of bond-strength disorder does indeed alter some of the vibrational properties of crystalline materials, compared to the introduction of structural disorder, it does not as readily destroy the crystalline- and Debye-like properties at low frequencies. Thus, at least within the present experimental regimes, it appears that structural order in crystalline materials is more important than bond homogeneity for maintaining crystalline phonon properties at low frequencies. This finding is superficially in conflict with previous simulation work on interaction disordered crystals, which have found a boson peak at low frequencies when enough disorder is present [45–49]. The previous simulation work examined a variety of spring constant distributions including a box distribution with plus/minus 20% variation about the average [45], truncated Gaussian distributions with widths varying from 0.6 to 1 [46, 48], power law distributions [47], and binary distributions with a spring constant ratio of 0.1 [47,49]. The simulations of binary distributions are closest to our experiments. However, these simulations started with a crystal of primarily hard springs and then doped it with soft springs. By contrast our experiments employed a soft crystal doped with hard particles. Also, the simulations used only two spring constants (soft and hard), whereas our experiments had three distinct spring constants (soft, hard, and intermediate stiffness), corresponding to our three interparticle interactions, i.e., soft-soft, hard-hard, and soft-hard, respectively. It should be interesting for future work to push to higher concentrations of hard spheres or to start with hard-particle crystals and add soft dopants. These experiments should be possible but are technically more difficult because the hard polystyrene particles scatter significantly more light than the PNIPAM particles, and tracking PNIPAM particles surrounded by a large number of polystyrene particles is difficult.

Looking to the future, it should be interesting to increase the bond-strength disparity by using softer particles. This variation, as well as the use of higher hard-particle concentrations, would enable us to probe systems closer to the onset of mechanical instability. The responses of these materials to mechanical perturbations would also be interesting to study. Given that colloidal glasses have been shown to possess quasilocalized "soft spots" that correlate with the location of structural rearrangements [24–30], it would be interesting to see when and if the soft spheres would become literal soft spots in hard crystals that facilitate rearrangements (due to

thermal motion or mechanical stress). Finally, in a different vein, these systems potentially offer a new class of so-called phononic materials in which localization of elastic energy (i.e., phonons) can influence wave transport [65,66].

ACKNOWLEDGMENTS

[1] G. L. Hunter and E. R. Weeks, Rep. Prog. Phys. **75**, 066501 (2012).

[2] P. N. Pusey, J. Phys.: Condens. Matter **20**, 494202 (2008).

[3] Z. H. Stachurski, Materials **4**, 1564 (2011).

[4] S. Schneider, J. Phys.: Condens. Matter **13**, 7723 (2001).

[5] M. D. Ediger, C. A. Angell, and S. R. Nagel, J. Phys. Chem. **100**, 13200 (1996).

[6] G. N. Greaves and S. Sen, Adv. Phys. **56**, 1 (2007).

[7] B. Frick and D. Richter, Science **267**, 1939 (1995).

[8] K. Chen, E. J. Saltzman, and K. S. Schweizer, J. Phys.: Condens. Matter **21**, 503101 (2009).

[9] M. van Hecke, J. Phys.: Condens. Matter **22**, 033101 (2010).

[10] C. Brito and M. Wyart, Europhys. Lett. **76**, 149 (2006).

[11] M. Wyart, Ann. Phys. **30**, 1 (2005).

[12] N. Xu, Front. Phys. China **6**, 109 (2011).

[13] G. Carini, G. D'Angelo, G. Tripodo, A. Fontana, A. Leonardi, G. A. Saunders, and A. Brodin, Phys. Rev. B **52**, 9342 (1995).

[14] L. Hong, B. Begen, A. Kisliuk, C. Alba-Simionesco, V. N. Novikov, and A. P. Sokolov, Phys. Rev. B **78**, 134201 (2008).

[15] Y. Inamura, M. Arai, T. Otomo, N. Kitamura, and U. Buchenau, Physica B **284-288**, 1157 (2000).

[16] R. O. Pohl, X. Liu, and E. Thompson, Rev. Mod. Phys. **74**, 991 (2002).

[17] H. Shintani and H. Tanaka, Nat. Mater. **7**, 870 (2008).

[18] S. Henkes, C. Brito, and O. Dauchot, Soft Matter **8**, 6092 (2012).

[19] L. E. Silbert, A. J. Liu, and S. R. Nagel, Phys. Rev. E **79**, 021308 (2009).

[20] P. M. Derlet, R. Maaß, and J. F. Löffler, Eur. Phys. J. B **85**, 148 (2012).

[21] P. Jund, D. Caprion, and R. Jullien, Phil. Mag. B **77**, 313 (1998).

[22] H. R. Schober, J. Phys.: Condens. Matter **16**, S2659 (2004).

[23] *Amorphous Solids: Low-Temperature Properties*, edited by W. A. Phillips (Springer-Verlag, Berlin, 1981).

[24] K. Chen, W. G. Ellenbroek, Z. Zhang, D. T. N. Chen, P. J. Yunker, S. Henkes, C. Brito, O. Dauchot, W. van Saarloos, A. J. Liu, A. G. Yodh, Phys. Rev. Lett. **105**, 025501 (2010).

[25] N. Xu, V. Vitelli, A. J. Liu, and S. R. Nagel, Europhys. Lett. **90**, 56001 (2010).

[26] K. Chen, M. L. Manning, P. J. Yunker, W. G. Ellenbroek, Z. Zhang, A. J. Liu, and A. G. Yodh, Phys. Rev. Lett. **107**, 108301 (2011).

[27] A. W. Cooper, H. Perry, P. Harrowell, and D. R. Reichman, J. Chem. Phys. **131**, 194508 (2009).

[28] A. Widmer-Cooper, H. Perry, P. Harrowell, and D. R. Reichman, Nat. Phys. **4**, 711 (2008).

[29] A. Tanguy, B. Mantisi, and M. Tsamados, Europhys. Lett. **90**, 16004 (2010).

[30] C. Brito and M. Wyart, J. Stat. Mech.: Theory Exp. (2007) L08003.

[31] K. Sun, A. Souslov, X. Mao, and T. C. Lubensky, Proc. Natl. Acad. Sci. USA **109**, 12369 (2012).

[32] H. S. Chen, H. J. Leamy, and C. E. Miller, Annu. Rev. Mater. Sci. **10**, 363 (1980).

[33] C. A. Angell, Science **267**, 1924 (1995).

[34] P. Yunker, Z. Zhang, and A. G. Yodh, Phys. Rev. Lett. **104**, 015701 (2010).

[35] A. Ghosh, V. K. Chikkadi, P. Schall, J. Kurchan, and D. Bonn, Phys. Rev. Lett. **104**, 248305 (2010).

[36] H. M. Lindsay and P. M. Chaikin, J. Chem. Phys. **76**, 3774 (1982).

[37] N. B. Simeonova and W. K. Kegel, Phys. Rev. Lett. **93**, 035701 (2004).

[38] P. N. Pusey and W. van Megen, Nature (London) **320**, 340 (1986).

[39] P. N. Pusey and W. van Megen, Phys. Rev. Lett. **59**, 2083 (1987).

[40] H. J. Schöpe, G. Bryant, and W. van Megen, J. Chem. Phys. **127**, 084505 (2007).

[41] E. R. Weeks, J. C. Crocker, A. C. Levitt, A. Schofield, and D. A. Weitz, Science **287**, 627 (2000).

[42] S. E. Phan, W. B. Russel, J. Zhu, and P. M. Chaikin, J. Chem. Phys. **108**, 9789 (1998).

[43] C. Patrick Royall, S. R. Williams, T. Ohtsuka, and H. Tanaka, Nat. Mater. **7**, 556 (2008).

[44] R. J. Elliott, J. A. Krumhansl, and P. L. Leath, Rev. Mod. Phys. **46**, 465 (1974).

[45] S. N. Taraskin, Y. L. Loh, G. Natarajan, and S. R. Elliott, Phys. Rev. Lett. **86**, 1255 (2001).

[46] W. Schirmacher, G. Diezemann, and C. Ganter, Phys. Rev. Lett. **81**, 136 (1998).

[47] J. W. Kantelhardt, S. Russ, and A. Bunde, J. Non-Cryst. Solids **307-310**, 96 (2002).

[48] W. Schirmacher, G. Diezemann, and C. Ganter, Physica B **263-264**, 160 (1999).

[49] W. Schirmacher and G. Diezemann, Ann. Phys. **8**, 727 (1999).

[50] A. M. Alsayed, Y. Han, and A. G. Yodh, *Microgel Suspensions* (Wiley-VCH, Weinheim, 2011), pp. 229–281.

[51] Y. Han, N. Y. Ha, A. M. Alsayed, and A. G. Yodh, Phys. Rev. E **77**, 041406 (2008).

[52] A. D. Dinsmore, A. G. Yodh, and D. J. Pine, Phys. Rev. E **52**, 4045 (1995).

[53] Z. Zhang, P. J. Yunker, P. Habdas, and A. G. Yodh, Phys. Rev. Lett. **107**, 208303 (2011).

[54] C. P. Royall, W. C. K. Poon, and E. R. Weeks, Soft Matter **9**, 17 (2013).

[55] See Supplemental Material at http://link.aps.org/supplemental/10.1103/PhysRevE.87.052301 for additional information on the

behavior of crystal subsections.

[56] J. Crocker, J. Colloid Interface Sci. **179**, 298 (1996).

[57] D. Kaya, N. L. Green, C. E. Maloney, and M. F. Islam, Science **329**, 656 (2010).

[58] C. Brito, O. Dauchot, G. Biroli, and J.-P. Bouchaud, Soft Matter **6**, 3013 (2010).

[59] M. Schindler and A. C. Maggs, Soft Matter **8**, 3864 (2012).

[60] A. Hasan and C. E. Maloney, arXiv:1212.4868 (2012).

[61] C. A. Lemarchand, A. C. Maggs, and M. Schindler, Europhys. Lett. **97**, 48007 (2012).

[62] Z. Burda, A. Görlich, A. Jarosz, and J. Jurkiewicz, Physica A **343**, 295 (2004).

[63] N. W. Ashcroft and N. D. Mermin, *Solid State Physics* (Harcourt College Publishers, Fort Worth, 1976).

[64] K. Chen, T. Still, K. B. Aptowicz, S. Schoenholz, M. Schindler, A. C. Maggs, A. J. Liu, and A. G. Yodh, arXiv:1212.1741 (2012).

[65] Z. Liu, X. Zhang, Y. Mao, Y. Y. Zhu, Z. Yang, C. T. Chan, and P. Sheng, Science **289**, 1734 (2000).

[66] T. Still, W. Cheng, M. Retsch, R. Sainidou, J. Wang, U. Jonas, N. Stefanou, and G. Fytas, Phys. Rev. Lett. **100**, 194301 (2008).